

Supplementary Information file for

**Oligomeric-Schiff bases as negative electrodes for Sodium Ion
Batteries: Unveiling the Nature of their Active Redox Centers**

María López-Herraiz ^a, Elizabeth Castillo-Martínez ^{a, *}, Javier Carretero-González ^{a, §},

Javier Carrasco ^a, Teófilo Rojo ^{a, b}, Michel Armand ^{a, *}

^a CIC EnergiGUNE, Alava Technology Park, C/Albert Einstein 48, 01510, Miñano,
Alava, Spain.

^b Departamento de Química Inorgánica, Universidad del País Vasco UPV/EHU, P.O.
Box 664, 48080 Bilbao, Spain.

[§] Current address: Polymer Ionics Research Group, Warsaw Technical University, 3
Noakowskiego, 00-664, Warsaw, Poland.

*Corresponding author: ecastillo@cicenergigune.com, michel.armand@gmail.com

1. Characterization of the Protonated Oligomers

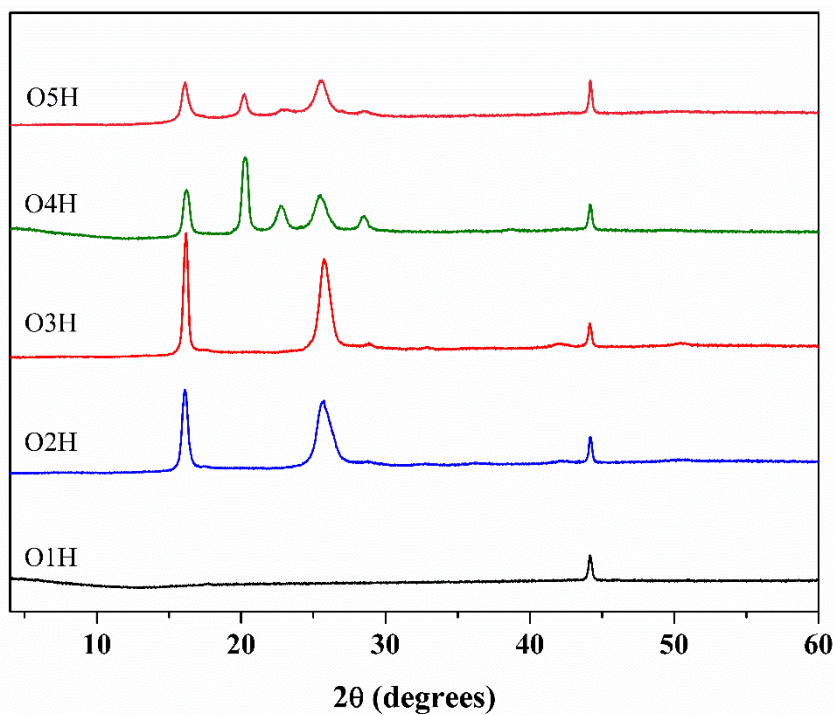


Figure S 1. PXRD patterns of the oligomers in their protonated form. (the sharp peak close to 45° corresponds to the steel sample holder)

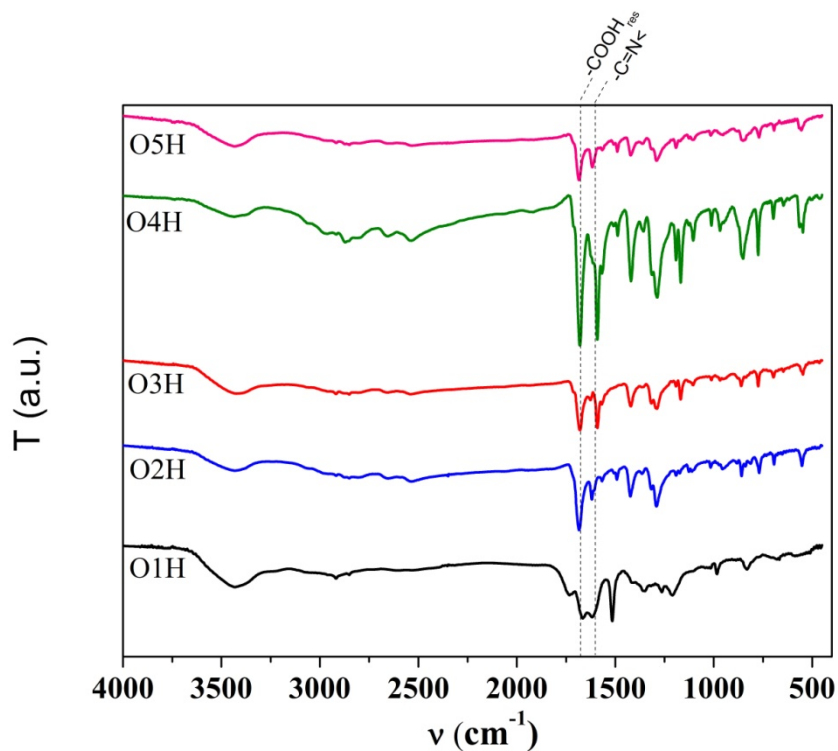


Figure S 2. IR spectra of the oligomers in their protonated form. The most characteristic carboxylate and imine bands are marked with dotted lines.

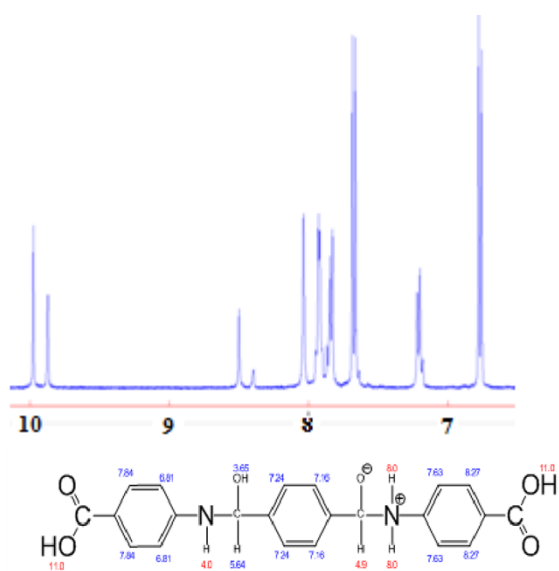
2. Solubility studies

Table S 1. Study of solubility performed for some of the oligomer Schiff-base.

	O1			O2Na			O3Na			O3H			O4Na			O5Na		
	RT	50°C	80°C	RT	50°C	80°C	RT	50°C	80°C	RT	50°C	80°C	RT	50°C	80°C	RT	50°C	80°C
H ₂ O	±	±	±	+			+			-	±	±	+			+		
EtOH _{25%} /H ₂ O 75%	-	-	±															
EtOH _{50%} /H ₂ O 50%	-	-	-															
EtOH _{75%} /H ₂ O 25%	-	-	-															
EtOH	-	-	-	-	-	-	-	-	-	-	-	-						
Toluene	-	-	-	-	-	-	-	-	-	-	-	-						
ACN	-	-	-	-	-	-	-	-	-	-	-	-						
Chloroform	-	-	-	-	-	-	-	-	-	-	-	-						
CH ₃ CO ₂ H	-	-	-	-	-	-	-	-	-	-	-	-						
DMSO	+			±	±	±	±	±	±				±	±	±	±	±	±
DMF	-	±	±	-	±	±	-	±	±				+			±		
NMP	-			±			±			-			±			±		

Soluble (+); partially soluble (±); insoluble (-); ACN= Acetonitrile; DMF = dimethylformamide; DMSO=**dimethylsulfoxide**; EtOH= Ethanol; **NMP=1-methyl-2-pyrrolidone**.

Due to the low solubility of the oligomers in all solvents except water, and being water susceptible to hydrolyze the imine bond, liquid NMR was performed for O2Na in D₂O. A certain degree of hydrolysis was observed, as the spectrum obtained is similar to the one simulated with Chemdraw for species with intermediate degrees of hydrolysis. Also, a mixture of the non-reacted initial species is also obtained as it is seen in Figure S 3.



Estimation quality is indicated by color: good, medium, rough

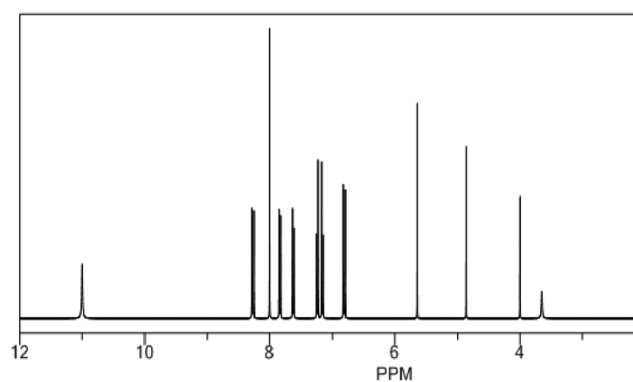


Figure S 3. Liquid 1H -NMR for O_2Na in D_2O (a) experimental results and (b) result simulated with Chemdraw software for O_2H which is being hydrolysed as shown in the molecule above.

3. Sodiated oligomers recrystallized from water.

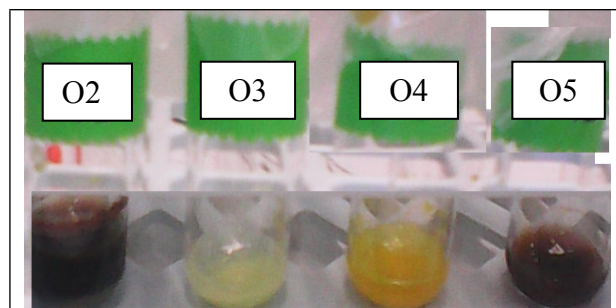


Figure S 4. Appearance of oligomers in their sodiated form after being for one day dissolved in water.

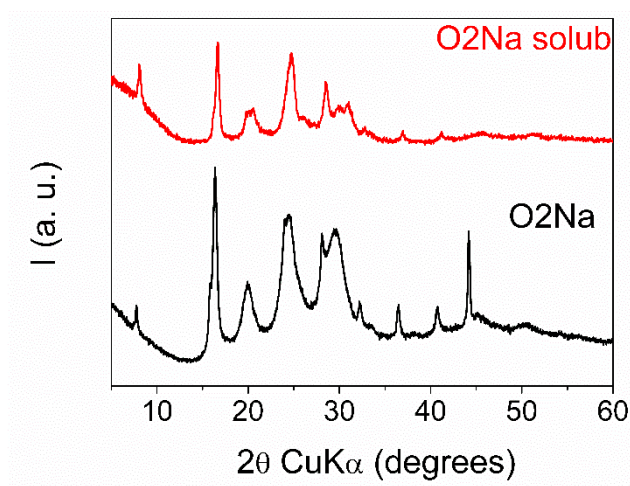


Figure S 5. PXRD pattern of O2Na after synthesis (black) and after recrystallization from water (red). The peak close to 45° corresponds to the sample holder.

4. Thermal stability of the oligomers.

The thermal properties of the oligomers were evaluated by Simultaneous Thermal Analysis (STA) combining Thermogravimetry (TGA) and differential scanning calorimetry (DSC) on each sample in a single instrument.

Representative TGA and DSC curves for all the oligomers are presented in Figure S 6 and Figure S 7 in air and in argon atmosphere respectively.

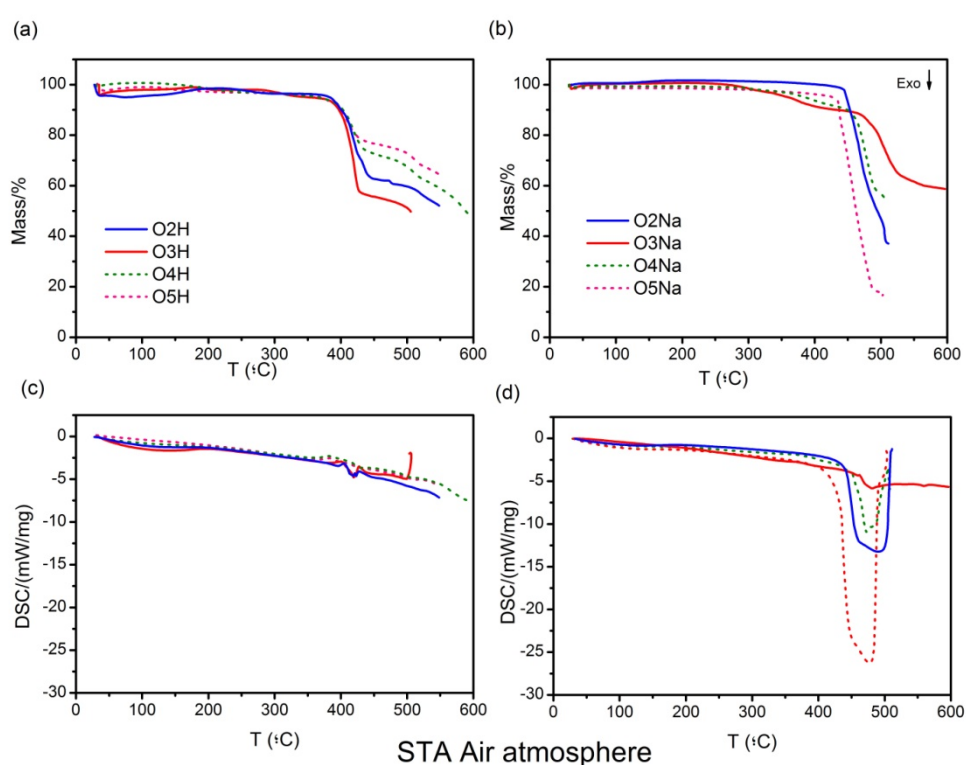


Figure S 6. TGA and DSC curves for all the oligomers in their protonated and sodiated forms under air atmosphere (60ml/min) at 10K/min. Note the different y-axis scales.

TG curves show that the oligomers have relatively good thermal stability with a mass loss of about 30-40%wt in their protonated form at about 390-410°C **Figure S 6a**. The loss of mass increases when the oligomers are in their sodiated form, up to 85% mass loss in the case of O5Na compared to a 25% in O5H, and this mass loss occurs at higher temperature. Therefore, it can be concluded that the sodiated form of all the monomers

is thermally more stable than in the protonated form. Probably it is due to stronger intermolecular interactions produced by Na^+ ions.

Oligomers O2-O5 in their protonated form, show an endothermic peak, Figure S 6c and 6d, at about 390-400°C, which probably corresponds to the melting temperature, as the recovered solid residue is stacked to the walls of the sample holder, reminiscent of its liquid state. On the other hand, oligomers in their sodiated form, do not melt but decompose at a temperature about 490-500°C, as observed on the DSC curve Figure S 6d.

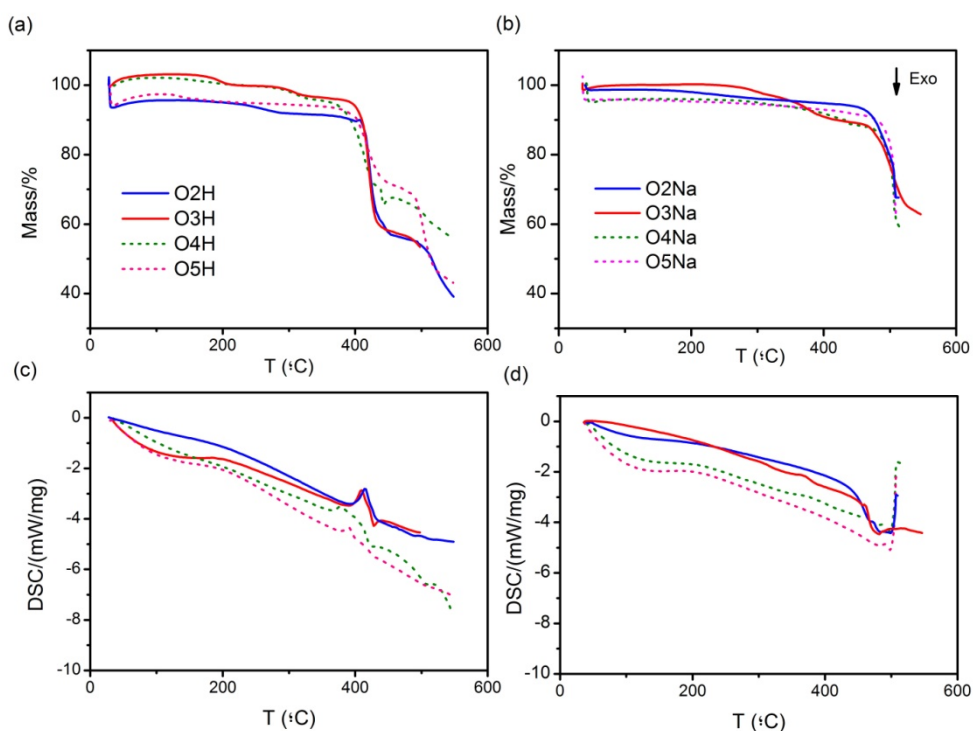


Figure S 7. TGA and DSC diagrams for the oligomers in their protonated and sodiated forms under argon atmosphere (60 ml/min) at 10K/min.

Similar behaviors are observed under argon atmosphere Figure S 7. The difference when using a more stable atmosphere, as it is the case of argon, is the decrease in the mass loss when heating, as the oligomers do not react with the atmosphere. There is no

additional CO₂ loss from CH reacting with O₂. The decomposition behavior of the oligomers is a bit complex and further investigation should be done.

5. Electrochemical performance

All the oligomers show at least one plateau in the studied voltage range, which means that they are all electrochemically active at the voltage desired for anodes operation in SIB.

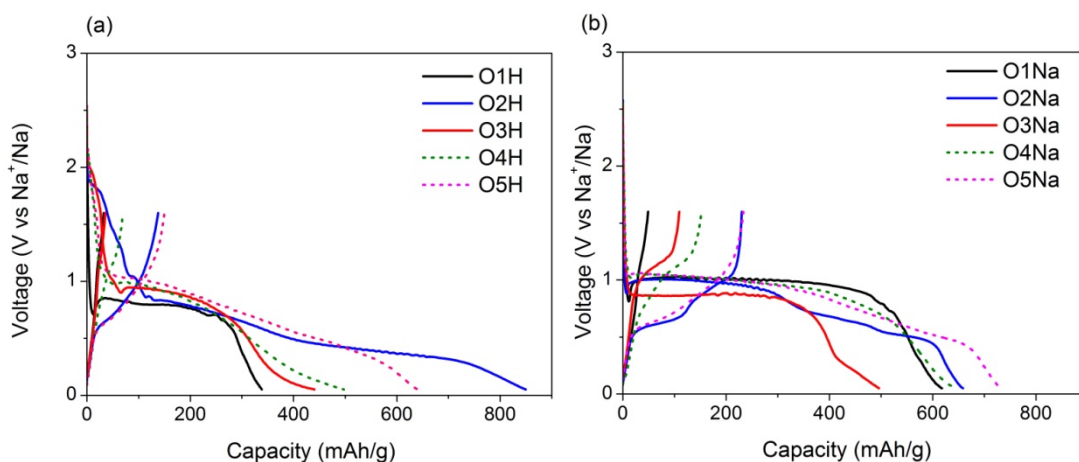


Figure S 8. Voltage vs. specific capacity for the 1st galvanostatic reduction and oxidation of OnH (a) and OnNa (b) mixtures with 15% carbon C-65 and 5% Ketjen black.

Capacities of 160 and 40 mAh/g for O2H and O3H respectively are achieved, even though they present the same PXRD pattern. The similar capacities for the discharge-charge imply that Na⁺ ions insertion and extraction are almost fully reversible. In the case of O2H, contrary to the case of O3H, this value is higher than its theoretical one, deducing that more than 2 Na⁺ ions are introduced into the oligomer unit while discharging.

Table S 2. Summary of most relevant electrochemical results.

Code	Theo. Cap Na ⁺ -C=N	Cap. 1st red.	Cap 1st oxid.	Na ⁺ /monomer unit	Ox/red1	Ox/red2	Ox/red3
------	--------------------------------	---------------	---------------	-------------------------------	---------	---------	---------

	mAh/g	mAh/g	mAh/g	V	V	V
O1H	186	340	32	0.6		1,2/0,8
O1Na	161	620	50	0.6		1,18/0,76
O2H	288	820	134	1.87	0,65/0,49	0,97/0,77 -
O2Na	258	660	268	3.97	0,62/0,53	0,90/0,75 1,01/0,85
O3H	288	420	35	0.50	-	1,19/0,78
O3Na	258	500	120	1.87	0,87/0,31	1,14/0,99
O4H	278	490	67	1.45	0,77/0,71	1,14/1,07
O4Na	258	640	150	3.53	0,81/0,79	1,08/0,98
O5H	278	640	150	3.22	0,65/0,56	0,99/0,80 1,19/1,02
O5Na	258	720	260	5.92	0,65/0,57	0,99/0,80 1,15/1,02

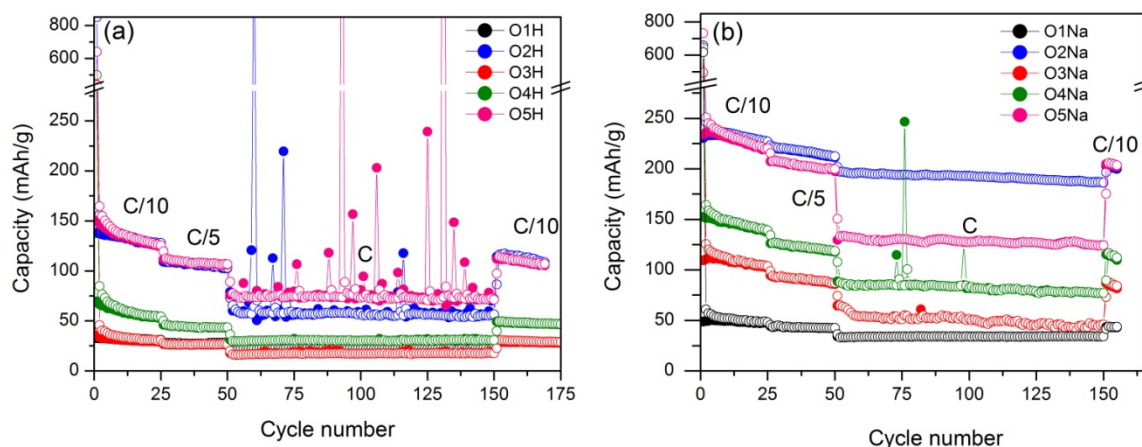


Figure S 9. Capacity vs Cycle number for OnH (a) and OnNa (b) mixtures with 15% carbon C-65 and 5% Ketjen black.

The cycle life of all protonated and sodiated oligomers is shown in **Figure S9**. The oligomers were cycled at C/10 for 25 cycles, C/5 for additional 25 cycles and 1C for 100 cycles with 1C corresponding to the current needed to charge/discharge the theoretical capacities as listed in Table S1 in 1 hour; i.e. $1\text{Na}^+/\text{C}=\text{N}$ or $\text{C}=\text{O}$. When cycling at high C-rates, in some instances, (O2H, O5H and O4Na) there are spikes in the charge capacity vs cycle number. We speculate that the spikes are due to formation of soft dendrites during sodium metal plating on the sodium counter electrode. These soft dendrites, which are very small and localized, might be temporarily short-circuiting

the cell until the next reduction starts. Therefore, they do not affect the battery performance irreversibly.

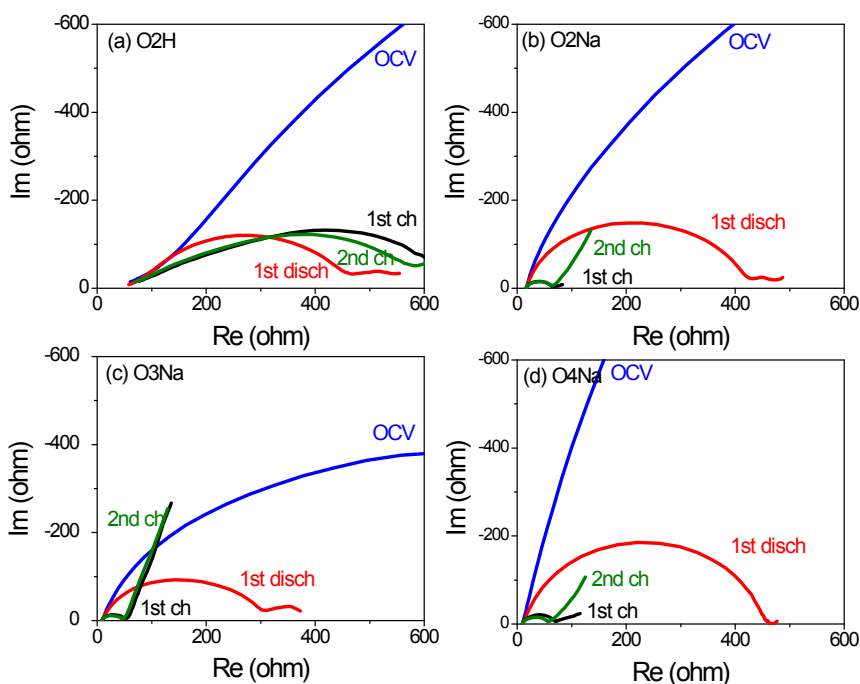


Figure S 10. Impedance plot for representative samples (a) O2H, (b) O2Na, (c) O3Na, (d) O4Na collected at: OCV after stable voltage (blue); at 0.005V vs Na^+/Na after the first discharge (red); at 1.6V vs Na^+/Na after the first charge (black) and at 1.6V vs Na^+/Na after the second charge.

Electrochemical Impedance Spectroscopy (EIS) data was collected in 2 electrode cells with a VMP potentiostat in the 500 kHz-100mHz frequency range. EIS data for representative materials are shown in **Figure S 10**. Data were collected at: OCV after stable voltage (blue curve); at 0.005V vs Na^+/Na after the first discharge (red); at 1.6V vs Na^+/Na after the first charge (black) and at 1.6V vs Na^+/Na after the second charge. When the oligomers are discharged the Nyquist plot show a semicircle which approach the x axis at resistances close to 400 ohm, which is related to the charge transfer resistance between the electrode and the electrolyte. After the first charge, all sodiated oligomers show a large drop in charge transfer resistance, with the intercept of the

semicircle with the x -axis falling below 100 ohm, whereas the protonated oligomer shows a slight increase to resistances larger than 500 ohm. Also, the shape of the curve is not a semicircle, implying that there are more than one process contributing to that resistance. Finally, the impedance plot remains almost constant after the second charge in all oligomers which agrees with all oligomers showing similar capacity fading with cycling.

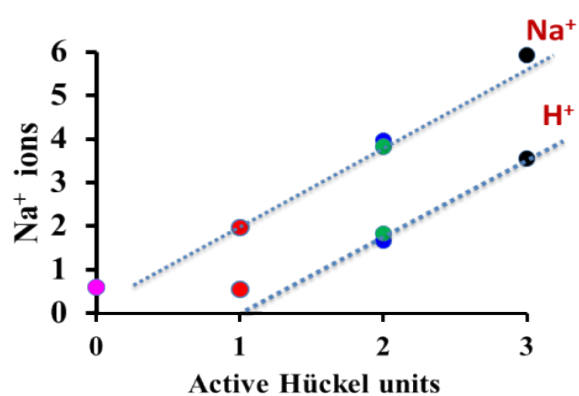


Figure S 11. Experimental relationship between Na^+ ions inserted and active Hückel units for all the oligomers in their protonated and sodiated forms.

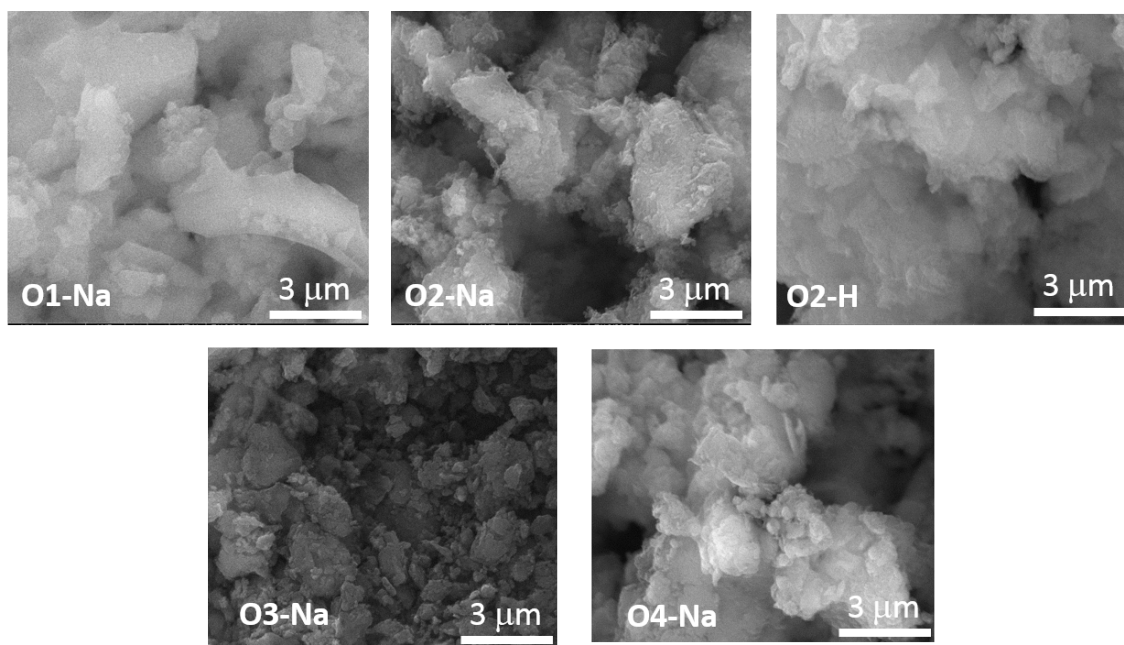


Figure S 12. SEM image of the oligomers O1-Na, O2-Na, O2-H, O3-Na and O4-Na.

Scanning electron microscopy (SEM) images were collected using a Quanta 250FEG (field emission gun) operated at 30kV. Given the insulating character of the materials, the oligomers had to be coated with a thin film of gold to allow imaging. The SEM images (Figure S 12) of the oligomers showed an irregular particle size for all powders, both protonated and sodiated.

6. Optimized Oligomers

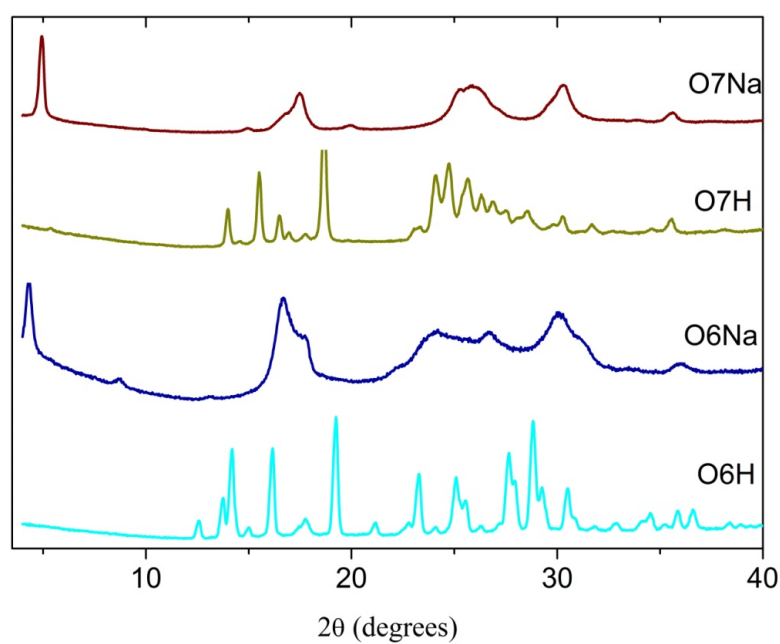


Figure S 13. *PXRD patterns of the O6 and O7 aza-oligomers in their protonated and sodiated forms.*

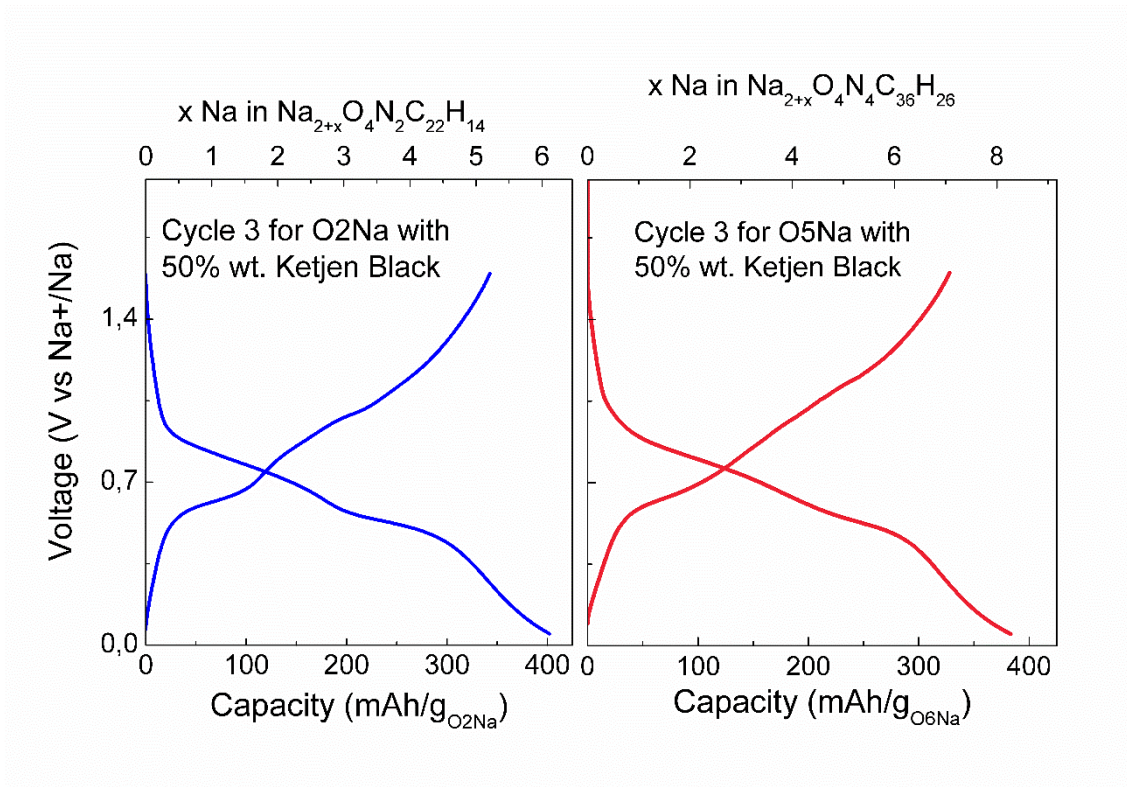


Figure S 14. Voltage vs specific capacity for the 3rd galvanostatic reduction and oxidation of O2Na and O6Na mixed with 50% wt. Ketjen black.

6. Density functional theory calculations

We performed density functional theory (DFT) calculations within the Vienna ab initio simulation package (VASP, version 5.3.3).¹⁻² We treated explicitly the H (1s), C (2s, 2p), N (2s, 2p), and O (2s, 2p) electrons as valence states expanded in plane-waves with a cutoff energy of 420 eV, whereas the remaining electrons were kept frozen as core states in the projector-augmented wave method.³ Total energies and electron densities were computed with the Perdew–Burke–Ernzerhof exchange-correlation functional.⁴ We used a (40×20×20) Å periodic box and Γ -point sampling. All atoms were allowed to fully relax using a conjugate-gradient algorithm with a residual force threshold of 0.01 eV/Å. Total energies were converged better than 10^{-6} eV per unit cell in each self-consistent field cycle. These computational settings guarantee a tight convergence in energies (<10 meV) and equilibrium distances (<0.01 Å).

Figure S 15 shows the optimized atomic structures of the most stable conformation of O2 and O3 gas-phase molecules. For O3 molecules, two distinct families of conformers were considered (*trans* and *cis*), which differ in the relative orientation of the two C=N bonds within the molecule. We explored the relative stability of different conformations as a function of the two dihedral C–N=C–C angles, α and β . Local minima in the potential energy surface exist at α and β angles of approximately 0°, 40°, 90°, 140°, 180°, 220°, 270°, and 320°. This corresponds to a total of 64 different conformations for each molecule. However, many of them are equivalent by symmetry. In **Table S 3** we give the optimized α and β angles for all non-equivalent conformations together with their relative energies with respect to the most stable O2 or O3 isomer. We notice that the relative orientation of the two terminal carboxylic groups within each molecule has a minor effect on total energies (<6 meV) and, therefore, we have not further considered

this extra degree of freedom. In addition, we explored the impact on stability of the dihedral angle ϕ (Figure 6 of main text), while keeping the C–C–N=C torsion in a planar configuration ($\alpha=0.6^\circ$). We found that preserving C–C–C=N planarity ($\phi\approx 0^\circ$ or $\phi\approx 180^\circ$) is energetically preferred. In Table S 4 we provide the Cartesian coordinates of the most stable structures for O2, *trans* O3, and *cis* O3 molecules shown in **Figure S 15**.

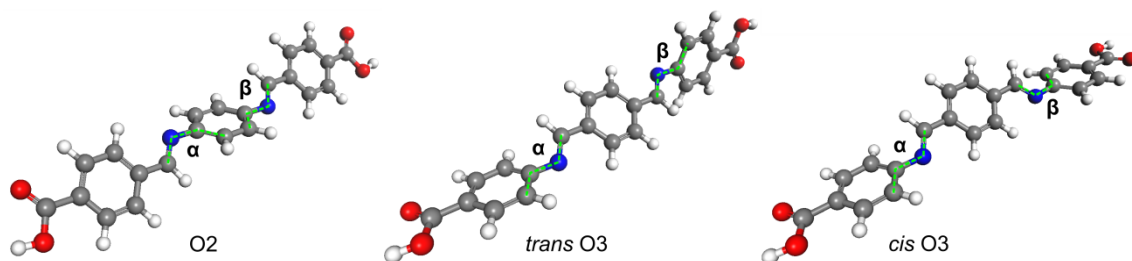


Figure S 15. Optimized structures of O2, *trans* O3, and *cis* O3 gas-phase molecules in their most stable conformation. Dihedral α and β angles are also shown. Color code: H, white; C, grey; N, blue; and O, red.

Table S 3. Optimized α and β angles (in degrees) for O2, *trans* O3, and *cis* O3 gas-phase molecules in different conformations. The relative energies (in meV) with respect to the most stable O2 or O3 isomers, E_r , are also given.

O2			<i>trans</i> O3			<i>cis</i> O3		
α	β	E_r	α	β	E_r	α	β	E_r
40.4	217.6	0	320.0	219.6	0	320.2	136.7	3
41.2	39.6	6	320.1	317.5	2	319.8	222.6	5
320.0	42.9	8	319.7	272.0	65	319.8	267.8	64
315.9	219.7	8	0.9	219.5	67	319.6	180.4	68
0.5	143.0	33	0.9	317.6	68	271.1	267.8	128
0.6	37.9	37	268.9	271.0	130	271.1	179.6	133
0.1	179.3	77	1.0	0.5	132	0.8	179.7	137
0.3	0.5	94	0.9	272.1	132			
215.5	87.0	101						
216.7	275.1	103						
90.2	3.2	129						
93.0	271.1	223						
89.6	92.6	230						

Table S 4. Optimized Cartesian coordinates of the most stable O2 and O3 isomers shown in **Figure S 15**.

Atom	O2			<i>trans</i> O3			<i>cis</i> O3		
	x	y	z	x	y	z	x	y	z
N	18.1046	9.6010	6.8478	18.0587	9.5094	7.0806	18.0613	9.5037	7.0840
N	23.7116	9.6796	7.2619	23.8024	9.5437	6.9328	23.7999	9.5899	6.8742
C	19.4956	9.6047	6.9842	19.5205	9.4990	7.0199	19.5215	9.4954	7.0095
C	20.2768	9.5263	5.8154	20.2555	8.2980	7.0089	20.2579	8.2903	6.9895
C	21.6631	9.5344	5.8864	21.6425	8.3309	6.9729	21.6405	8.3125	6.9354
C	22.3195	9.6556	7.1301	22.3398	9.5566	6.9476	22.3383	9.5401	6.8999
C	21.5387	9.7307	8.2993	21.6048	10.7575	6.9522	21.6059	10.7399	6.9151
C	20.1515	9.7202	8.2287	20.2176	10.7246	6.9877	20.2152	10.7176	6.9689
C	13.0977	8.9813	7.5904	13.1476	8.4350	7.2259	25.9186	8.6001	6.8457
C	13.7866	8.1428	8.4802	13.8903	7.5941	8.0734	26.6198	9.4570	5.9717
C	15.1778	8.1546	8.5038	15.2779	7.6032	8.0289	28.0114	9.4575	5.9544
C	15.9060	8.9912	7.6389	15.9627	8.4800	7.1637	28.7333	8.6108	6.8119
C	15.2069	9.8288	6.7465	15.2138	9.3156	6.3070	28.0352	7.7455	7.6721
C	13.8204	9.8239	6.7256	13.8249	9.2872	6.3387	26.6492	7.7251	7.6757
C	17.3679	8.9648	7.6903	11.6659	8.4470	7.2170	30.2140	8.5752	6.8435
C	24.4259	10.3464	6.4229	25.9048	10.5551	6.8934	13.1545	8.4340	7.2271
C	25.8876	10.3647	6.4607	26.6492	11.4336	7.7061	13.8935	7.5902	8.0752
C	26.6230	9.5492	7.3428	28.0375	11.4194	7.6756	15.2813	7.5963	8.0342
C	28.0100	9.6120	7.3640	28.7196	10.5516	6.8043	15.9689	8.4726	7.1709
C	28.6929	10.4942	6.5055	27.9814	9.7002	5.9663	15.2238	9.3103	6.3131
C	27.9661	11.3035	5.6196	26.5929	9.6967	6.0087	13.8352	9.2856	6.3421
C	26.5786	11.2342	5.5959	30.1982	10.5053	6.7214	11.6731	8.4505	7.2150
C	11.6144	9.0201	7.5240	17.3588	8.4316	7.1571	17.3644	8.4241	7.1632
C	30.1734	10.6130	6.4969	24.5107	10.6187	6.9636	24.5253	8.5270	6.8983
H	19.7670	9.4303	4.8554	19.7138	7.3519	7.0370	19.7114	7.3471	7.0252
H	22.2542	9.4196	4.9763	22.2095	7.3967	6.9700	22.2184	7.3876	6.9279
H	22.0486	9.8297	9.2590	22.1466	11.7037	6.9343	22.1374	11.6942	6.8914
H	19.5600	9.8345	9.1387	19.6507	11.6589	6.9965	19.6528	11.6541	6.9863
H	13.2282	7.4873	9.1473	13.3695	6.9252	8.7578	17.5834	10.5023	7.0966
H	15.7166	7.5031	9.1959	15.8634	6.9431	8.6697	24.2517	10.6008	6.8705
H	15.7779	10.4768	6.0808	15.7322	9.9586	5.5936	26.0641	10.0964	5.2836
H	13.2634	10.4694	6.0456	13.2351	9.9198	5.6738	28.5493	10.1141	5.2706
H	17.8106	8.3373	8.4876	17.5834	10.5093	7.0890	28.6085	7.0865	8.3250
H	23.9600	10.9747	5.6398	24.2742	8.5422	6.9238	26.0979	7.0465	8.3274
H	26.0809	8.8732	8.0048	10.1480	7.6727	8.0252	31.7602	9.3296	6.0760
H	28.5788	8.9800	8.0453	26.1105	12.1126	8.3679	13.3694	6.9216	8.7574
H	28.5120	11.9809	4.9623	28.6056	12.0892	8.3203	15.8640	6.9346	8.6758
H	26.0116	11.8653	4.9076	28.5239	9.0475	5.2809	15.7462	9.9515	5.6010
H	10.0529	8.2741	8.2732	26.0260	9.0541	5.3330	13.2484	9.9205	5.6767
H	31.7433	9.9482	7.3011	31.7725	11.2547	7.4390	10.1509	7.6809	8.0189
O	10.9634	9.7324	6.7719	10.9688	9.1469	6.4933	30.8857	7.8579	7.5743
O	11.0168	8.1612	8.4074	11.1179	7.5763	8.1234	30.7945	9.4453	5.9573
O	30.8129	11.3682	5.7769	30.8416	9.7756	5.9776	10.9799	9.1535	6.4905
O	30.7827	9.7799	7.3959	30.8113	11.3781	7.5826	11.1202	7.5808	8.1192

7. Density estimations

We have calculated the hypothetical theoretical density for protonated oligomers based on the Van der Waals volume contributions for polymers⁵ and the known molecular weights. (Table S 5) Calculated densities are in the 1.42-1.68 g/cm³. Slightly higher

densities are expected for the sodiated oligomers. This is to be compared with $\approx 2 \text{ g/cm}^3$ for carbonaceous materials among which hard carbon with a lower specific capacity and a relatively unsafe voltage zone too close to Na° plating

Table S 5. Calculated theoretical densities based on the additive contributions of groups for polymers. Van der Waals Group values according to Bondi and Slomiskii are: 43.32 and 45.2 g/mol for $-\text{C}_4\text{H}_6-$; 15.2 and 17 for $-\text{COO}-$; 16,94 and 18,1 for $-\text{CH}=\text{CH}-$; 29,25 for $-\text{C}\equiv\text{N}$ respectively. The value for $-\text{C}\equiv\text{N}$ is estimated as 1.5 times the value of V_g in table 4.6 of ref. S6. The value for $-\text{C}=\text{N}-$ (which is the actual unit in the oligomers) is estimated as the average of $-\text{CH}=\text{CH}-$ and that of $-\text{C}\equiv\text{N}$.

Oligomer	Number of units	V_w -Bondi (g/cm^3)	V_w -Slonimskii (g/cm^3)	M.W. (g/mol)	r(g/cm^3) Bondi	r(g/cm^3) Slomiskii
O1H	1Ph-2COO-2CHN	124,45	130,75	220	1,68	1,68
O2H/O3H	3Ph-2COO-4CHN	261,82	272,7	402	1,47	1,47
O4H/O6H	5Ph-2COO-6CHN	399,19	414,65	588	1,42	1,42

S.1 Kresse, G.; Hafner, J. Ab-Initio Molecular-Dynamics for Liquid-Metals. Phys. Rev. B 1993, 47, 558–561.

S.2 Kresse, G.; Furthmüller, J. Efficiency of Ab-Initio Total Energy Calculations for Metals and Semiconductors using a Plane-Wave Basis Set. Comput. Mater. Sci. 1996, 6, 15–50.

S.3 Kresse, G.; Joubert, D. From Ultrasoft Pseudopotentials to the Projector Augmented-Wave Method. Phys. Rev. B 1999, 59, 1758–1775.

S.4 Perdew, J.; Burke, K.; Ernzerhof, M. Generalized Gradient Approximation Made Simple. Phys. Rev. Lett. 1996, 77, 3865–3868.

S.5 Properties of Polymers. Correlations with Chemical Structure, by D.W. Van Krevelen, Elsevier Publishing Company, 1972. Table 4.8, p.50